The Cospectral Gap and Turbulent Flux Calculations

DEAN VICKERS AND L. MAHRT

College of Oceanic and Atmospheric Sciences, Oregon State University, Corvallis, Oregon

(Manuscript received 27 February 2002, in final form 30 October 2002)

ABSTRACT

An alternative method to Fourier analysis is discussed for studying the scale dependence of variances and covariances in atmospheric boundary layer time series. Unlike Fourier decomposition, the scale dependence based on multiresolution decomposition depends on the scale of the fluctuations and not the periodicity. An example calculation is presented in detail.

Multiresolution decomposition is applied to tower datasets to study the cospectral gap scale, which is the timescale that separates turbulent and mesoscale fluxes of heat, moisture, and momentum between the atmosphere and the surface. It is desirable to partition the flux because turbulent fluxes are related to the local wind shear and temperature stratification through similarity theory, while mesoscale fluxes are not. Use of the gap timescale to calculate the eddy correlation flux removes contamination by mesoscale motions, and therefore improves similarity relationships compared to the usual approach of using a constant averaging timescale.

A simple model is developed to predict the gap scale. The goal here is to develop a practical formulation based on readily available variables rather than a theory for the transporting eddy scales. The gap scale increases with height, increases with instability, and decreases sharply with increasing stability. With strong stratification and weak winds, the gap scale is on the order of a few minutes or less. Implementation of the gap approach involves calculating an eddy correlation flux using the modeled gap timescale to define the turbulent fluctuations (e.g., w' and T'). The turbulent fluxes (e.g., $w'T'$) are then averaged over 1 h to reduce random sampling errors.

1. Introduction

Our purpose is twofold: to (i) study the cospectral gap that separates turbulent and mesoscale contributions to the calculated fluxes of heat, moisture, and momentum; and (ii) present a description of multiresolution decomposition including a simple example. Multiresolution analysis applied to time series decomposes the record into averages on different time scales and represents the simplest possible orthogonal decomposition. Multiresolution (MR) spectra yield information on the scale dependence of the variance as do Fourier spectra, but unlike Fourier spectra, MR spectra satisfy Reynold's averaging at all scales and do not assume periodicity (Howell and Mahrt 1997). The location of the peak of MR spectra in the time scale domain depends primarily on the timescale of the fluctuations, while the peak of Fourier spectra depends on the periodicity. Howell and Mahrt (1997) found that Fourier spectra tend to be shifted to larger scales because local MR spectra respond to event widths, whereas the global Fourier spectra are influenced by the time between events. Multiresolution spectra can be interpreted in terms of (i) using simple unweighted moving averages (the approach presented here), (ii) the Haar transform method (Haar 1910; Howell and Mahrt 1997), and (iii) wavelets (Mallat 1989; Katul and Vidakovic 1996). The multiresolution basis set is a wavelet basis set with a constant basis function, and is the only basis set that satisfies Reynold's averaging.

Eddy correlation flux calculations from tower data require the researcher to choose a timescale τ (or a length scale for aircraft data) to define the fluctuations. The calculated flux includes all scales of motion from the smallest resolved by the instrumentation up to the specified averaging timescale τ, and therefore, the calculated flux depends on the choice of τ. Since the atmosphere typically contains motions and coherent vertical transports (fluxes) on a wide range of timescales, the selection of τ is not always straightforward. The choice of τ varies in the literature, where a typical value is 30 min. Differences in τ may contribute to some of the differences between studies, especially for the stable boundary layer. The choice of τ may be influenced by the goal of the particular research. For example, while studying similarity relationships, one might attempt to remove all nonturbulent contributions to the fluxes, while for balancing surface energy budgets one might want to include heat fluxes at larger timescales, regardless of their origins.

Corresponding author address: Dean Vickers, College of Oceanic and Atmospheric Sciences, Oceanography Administration Bldg. 104, Oregon State University, Corvallis, OR 97331-5503.
E-mail: vickers@coas.oregonstate.edu

The scale dependence of the flux often reveals a cospectral gap region that separates the turbulent scales of the cospectra from the mesoscale transport (Smedman and Högström 1975; Stull 1990). These mesoscale flows can include deep convection, large roll vortices and local circulations due to topographical or surface heterogeneity. In stable flows, mesoscale motions can include internal gravity waves, drainage flows, and other less well known motions. Wave-turbulence interactions at timescales as small as a few hundred seconds have been observed to cause both gradient and countergradient heat fluxes in very stable conditions (Smedman 1988; Sun et al. 2002). Mahrt et al. (2001) found a spectral gap delineating turbulence and mesoscale motions by examining MR spectra (variances) of the wind components for a variety of different tower datasets. Howell and Sun (1999) used MR cospectra of the heat flux and a random flux sampling error criteria to determine a turbulence cutoff timescale for the stable boundary layer.

When relating fluxes to the local mean wind shear and temperature stratification, as in similarity theory, the prescribed timescale τ would ideally include transports on all turbulence timescales and exclude all mesoscale and larger motions. Mesoscale motions do not obey similarity theory and are poorly sampled on time scales of a few hours or less (Mahrt et al. 2001). Including mesoscale transport in calculated fluxes potentially degrades similarity relationships (Smedman 1988). This degradation is expected to be most significant for stable conditions, where the turbulent fluxes are small and inclusion of the mesoscale contribution can dramatically change the magnitude and even the sign of the calculated flux. In unstable conditions the turbulent flux is much larger, and therefore inadvertent inclusion of mesoscale transport is thought to have less impact on the calculated flux.

In this study, we address the issue of selecting a timescale for eddy correlation flux calculations that includes the turbulence but excludes the mesoscale. Multiresolution decomposition is used to examine the scale dependence of the momentum flux and the heat flux for tower datasets over relatively flat, homogeneous surfaces with low vegetation. The multiresolution decomposition method and a straightforward algorithm for calculating spectra and cospectra are presented in section 2. A discussion of the data is included in section 3. In section 4, the decomposition is applied to turbulence data to identify and model the cospectral gap region separating the contributions from turbulent and mesoscale motions to the calculated eddy correlation flux. We compare fluxes and similarity relationships using the new gap scale model to those calculated using the traditional approach of a constant averaging timescale in section 5.

2. Multiresolution decomposition

Consider a time series w_i consisting of $i = 1, 2 \cdots 2^M$ points. A method for mapping the series for an arbitrary number of points N onto 2^M points is outlined below. Multiresolution decomposition partitions the record into simple averages on different scales (segments) of width 1, 2, 4, . . . 2^M consecutive data points. The lowest order mode (largest scale) is the simple average over the record, which is then removed (Fig. 1a). The next mode consists of the means of the two half records (Fig. 1b), which are then removed. The third mode consists of the averages of the four subrecords, and so forth. This procedure can be thought of as a highpass filter that, with each application, removes increasingly shorter averaging timescale fluctuations.

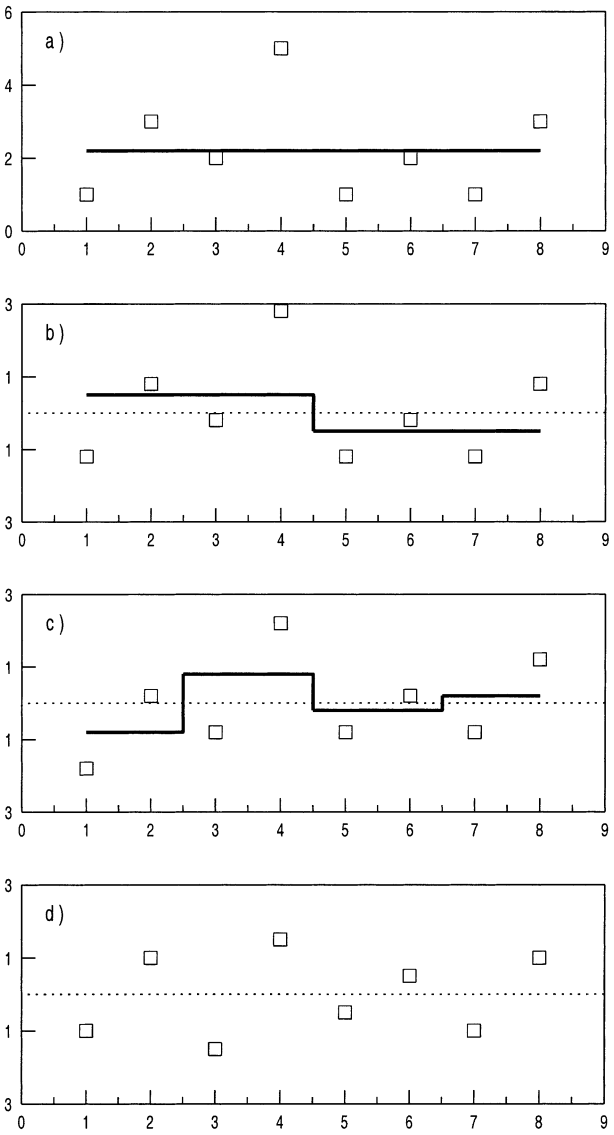

FIG. 1. Steps in multiresolution decomposition.

For a given scale m, the averaging segments of width 2^m points are sequenced as $n = 1, 2 \cdots 2^{M-m}$, where n identifies the position of the segment within the series. The average for the nth segment at scale m is given by

TABLE 1. Multiresolution orthogonal decomposition method applied to the time series with eight samples in Fig. 1.

m	$wr_i(m)$	$\overline{w}_n(m)$	MR spectra $(m + 1)$
3	1.00 3.00 2.00 5.00 1.00 2.00 1.00 3.00	2.25	—
2	−1.25 0.75 −0.25 2.75 −1.25 −0.25 −1.25 0.75	0.50 −0.50	0.25
1	−1.75 0.25 −0.75 2.25 −0.75 0.25 −0.75 1.25	−0.75 0.75 −0.25 0.25	0.3125
0	−1.00 1.00 −1.50 1.50 −0.50 0.50 −1.00 1.00	—	1.125

$$\overline{w}_n(m) = \frac{1}{2^m}\sum_{i=I}^{J} wr_i(m), \tag{1}$$

where $wr_i(m)$ is the residual series with segment averages for windows of width $>2^m$ points removed. The $wr_i(M)$ is the original series w_i. In Eq. (1), $I = (n - 1)2^m + 1$ and $J = n2^m$. In this notation, the lowest order mode (largest averaging timescale) corresponds to $m = M$, while the highest order mode (shortest averaging timescale) corresponds to $m = 0$.

The MR spectra are the second moment about the mean of the segment averages, given by

$$D_w(m + 1) = \frac{1}{2^{M-m}}\sum_{n=1}^{2^{M-m}} \overline{w}_n^2(m), \tag{2}$$

since the record mean of the segment averages is zero. To calculate MR cospectra for two time series w and ϕ, the same averaging and reduction procedures are applied as discussed above for MR spectra except that there are two time series and the cospectra are given by

$$D_{w\phi}(m + 1) = \frac{1}{2^{M-m}}\sum_{n=1}^{2^{M-m}} \overline{w}_n(m)\overline{\phi}_n(m). \tag{3}$$

The sum of $D_{w\phi}(m)$ over averaging scales $m = 1, P$ is precisely equal to the average eddy correlation flux calculated using an averaging scale of 2^P points,

$$\sum_{m=1}^{P} D_{w\phi}(m) = [(w - \overline{w}^P)(\phi - \overline{\phi}^P)], \tag{4}$$

where the overbar refers to a 2^P-point local averaging scale and the square brackets denote the record mean. The record length (2^M points) determines the time period over which the estimates of the flux are averaged. When $P = M$ there is a single timescale and the relationship between the MR cospectra and the eddy correlation flux simplifies to

$$\sum_{m=1}^{M} D_{w\phi}(m) = [(w - [w])(\phi - [\phi])]. \tag{5}$$

The right-hand side of Eq. (5) is the traditional Reynolds flux.

Fourier decomposition imposes periodic basis functions, and therefore an explicit relationship between Fourier spectra and MR spectra, or between Fourier spectra and Reynold's averaging, does not exist. The correspondence between our MR spectra notation and Fourier spectra is

$$D_w(m) \sim fS_w(f) = \kappa F_w(\kappa), \tag{6}$$

where we use the notation of Kaimal and Finnigan (1994) for the frequency-weighted (fS_w) and wavenumber-weighted (κF_w) forms of the Fourier spectrum. The MR spectra and the two weighted forms of the Fourier spectra in Eq. (6) have units of variance. The frequencies and wavenumbers associated with the MR spectra averaging timescales are $f = (\delta t 2^m)^{-1}$, $m = 1, M$, and $\kappa = f/U$, respectively, where δt is the time interval (s) between data points and U is mean wind speed (m s^{-1}). Normalized MR spectra are given by

$$G_w(n) = \frac{D_w(n)}{\sum D_w} \tag{7}$$

such that $G_w(n)$ is the fraction of the vertical velocity variance associated with normalized frequency n, where $n = fz/U$.

a. Example calculation

An example of the calculations for the time series in Fig. 1 is shown in Table 1. First, Eq. (1) is applied with $m = M = 3$ to the original series $wr_i(3)$. The segment averaging scale of 8 points yields $\overline{w}_1(3) = 2.25$ (line in Fig. 1a). This average is removed from all points in the series $wr_i(3)$ to yield the new residual time series $wr_i(2)$ (squares in Fig. 1b). Second, Eq. (1) is applied with $m = M - 1 = 2$ with a segment width of 4 points yielding $\overline{w}_1(2) = 0.5$ and $\overline{w}_2(2) = -0.5$. The MR spectra is calculated as the second moment about the mean of the $\overline{w}_n(2)$, which in this case gives $D_w(3) = 0.25$. The first segment average $\overline{w}_1(2)$ is removed from all points in the residual series $wr_i(2)$ within the $n = 1$ segment, and the second segment average $\overline{w}_2(2)$ is removed from all points in the $n = 2$ segment to give the new residual series $wr_i(1)$ (squares in Fig. 1c). Third, Eq. (1) is applied with $m = M - 2 = 1$ with a segment width of 2 points and the MR spectra is calculated using Eq. (2) yielding $D_w(2) = 0.3125$. The segment averages are removed from $wr_i(1)$ to produce $wr_i(0)$. For $m = 0$, the segment width is a single point, and $\overline{w}_n(0) = wr_i(0)$. Applying Eq. (2) yields $D_w(1) = 1.125$. This completes the decomposition. Here, $D_w(1)$ is the variance of w_i associated with an averaging time scale of 2^1 data points, $D_w(2)$ is for a scale of 2^2 points, and $D_w(3)$ is the variance associated with the largest scale of 2^3 points. The sum of $D_w(m)$, $m = 1, 2, 3$, is equal to the second moment of w about the record mean. Software that performs the decomposition is available from the author upon request. The code is available in Fortran77, c, Matlab, and IDL languages.

b. Mapping to 2^M points

The orthogonal decomposition requires that the time series consist of precisely 2^M samples. An original series of arbitrary length N is interpolated onto a new series of length 2^M, where M is the largest integer such that $2^M < N$. The time interval between samples of the new series of length 2^M is

$$\delta t = \frac{(N - 1)\delta t_o}{(2^M - 1)}, \tag{8}$$

where δt_o is the time interval of the original series and $\delta t > \delta t_o$. Linear interpolation between the two nearest points in the original series is used to calculate each point in the new time series. With this approach, all the data points in the original series are used. An alternative might be to select some portion of the original series and discard the remaining portion.

3. Data

The primary tower data is from the Cooperative Atmosphere–Surface Exchange Study–1999 (CASES99) grassland site in Kansas during October (Poulos et al. 2002). This dataset includes 16 different sonic anemometers of either Campbell CSAT or ATI K-probe design, deployed on 9 different towers tightly clustered in a circular region of diameter 600 m centered on a main 60-m tower. The sonics were deployed at a number of vertical levels ranging from 0.5–55 m above ground. We include sonic data from levels of 10, 20, 30, 40, 50 and 55 m on the NCAR ATD main 60-m tower; the UConn mini tower located 10 m to the side of the main tower with CSAT sonic anemometers at 0.5, 1.5, and 5 m; the Iowa flux tower with sonic anemometers at 1.5 and 5 m; and from the NCAR ATD network of 6 stations surrounding the main tower site each with a sonic anemometer at 5 m. The lower sonic level on the UConn tower was changed from 1.5 to 0.5 m during the experiment. Sonic pathlength averaging may influence the fluxes at the lowest deployment levels (below 2 m) where a larger fraction of the flux is carried by eddies with length scales which are not large compared to the pathlength (10 cm).

We obtained one month of 20-Hz time series data for all 16 of these CASES99 sonics. For the cospectra calculations, we consider individual time series of 1-h lengths. Flow through the tower and transition periods just after sunrise and sunset were excluded. A small amount of data were excluded based on the flux nonstationarity parameter following Mahrt (1998). The most nonstationary periods were discarded. A larger amount of data were discarded based on quality control testing (Vickers and Mahrt 1997). The most frequent cause of discarded data was flow through the tower structure prior to reaching the sensors.

Auxiliary tower datasets include (i) three Kaijo Denki sonic anemometers at 2, 10, and 20 m, and a Gill Solent sonic at 7 m above ground over a low heather canopy in the Borris Moor of Jutland in Denmark for one week in July 1995 (BORRIS95); and (ii) two ATI K-probe sonic anemometers at 3 and 10 m above Kansas grassland during March 1995 (MICROFRONTS). We use the auxiliary tower datasets to test the generality of the conclusions based on CASES99 results.

A tilt correction (e.g., Kaimal and Finnigan 1994), was applied to all of the above mentioned sonic anemometer data. Our tilt correction (Mahrt et al. 2000) is constructed by computing a practice tilt angle that eliminates the mean vertical motion for each 1-h record. After eliminating outliers, the average of the tilt angle is computed for each wind direction group of width 15° for all records with wind speeds exceeding 2 m s^{-1}. The directionally dependent tilt correction is then applied to all of the data, regardless of wind speed. Our tilt correction does not force the mean vertical motion to be zero for any individual 1-h period. Our procedure also searches for a nonzero, and possibly time-dependent offset in the mean vertical wind. If an offset is found, it is removed from the data before calculating and averaging the practice vertical tilt angles.

For the purpose of characterizing the stability dependence of the cospectral gap scale in the next section, we prefer the bulk Richardson number to z/L. Here R_b is independent of the fluxes, while the Obukhov length L is defined by the fluxes. Calculating an eddy correlation flux using a z/L dependent averaging time scale could be difficult to implement for all flow situations and would require an iterative approach since z/L would depend on the averaging timescale, which would depend on z/L, and so forth. Instead, we use a bulk Richardson number calculated as

$$R_b = \frac{(\theta_z - \theta_{\text{sfc}})gz}{\theta_z U_z^2}, \tag{9}$$

with $z = 15$ m and where θ_{sfc} is the 1-h average surface radiative temperature based on measurements made at the six stations in the ATD CASES99 network. Using surface radiative temperature measurements over land is often problematic due to irregularities in surface cover and differences between the radiometer footprint and the flux footprint. However, in CASES99, these problems are reduced by averaging the radiative temperature estimates from six different locations all with similar surfaces (grassland). Here, U_z is taken as the vector average wind speed from an R.M. Young propeller vane anemometer at 15 m on the main tower, and the air temperature θ_z is taken from the ATD aspirated and shielded temperature measurement at 15 m on the main tower. Over 90% of the 1-h average bulk Richardson numbers in CASES99 are in the range -1 to 1 (Fig. 2).

For the BORRIS95 dataset, we calculated R_b using the temperature difference between thermocouples at 0.23 and 16.3 m above ground and the wind speed from a sonic anemometer at 20 m. For MICROFRONTS, the

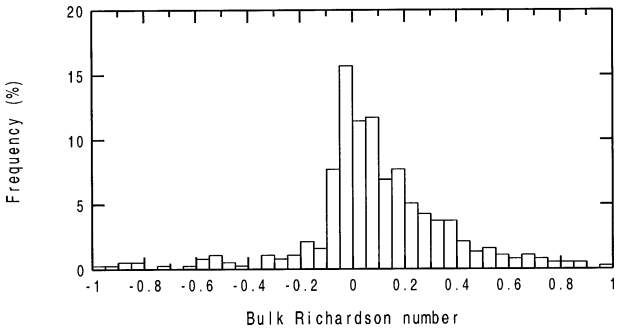

FIG. 2. Frequency distribution of the bulk Richardson number in CASES99 for 376 1-h periods.

gradients were based on the temperature difference between ATD aspirated and shielded sensors at 2 and 10 m and the wind speed from a 10-m propeller vane.

4. Cospectral gap scale

The cospectral gap scale was examined by studying MR cospectra of the momentum and heat flux for each 1-h period. We chose 1 h as a compromise. Longer time periods are desirable to reduce random sampling errors, while shorter periods reduce the influence of nonstationarity. In most stable cases, a gap region was clearly evident in the MR cospectra. The fluxes of heat and momentum at timescales larger than the gap scale are often erratic, a strong function of averaging time and can be of either sign, and unlike the turbulent scale fluxes, have no clear relationship to the local shear or stratification (Fig. 3). For averaging times shorter than a few minutes, downward heat flux is nearly always present in the stable boundary layer. A gap region was not always evident for unstable periods where the distinction between large convective eddies that scale with boundary layer depth and mesoscale motions becomes blurred. The large difference in the spatial scales of turbulent transport between unstable and stable conditions is due to augmentation of the large eddies by convection and suppression of the large eddies by stable stratification.

An automated algorithm was developed to objectively find the gap timescale. The algorithm scans the MR cospectra [Eq. (3)] beginning with the shortest averaging timescale and progressing to longer timescales. The first peak in the cospectra is identified by a decrease in magnitude with increasing scale and is associated with turbulence. The gap between turbulence and mesoscale motions is identified when the cospectra either increase or level off at an averaging time scale longer than the scale associated with the turbulence peak. A leveling off is identified when the accumulative flux changes by 1% or less with an increase in timescale. Individual cospectra for 1-h time series are first smoothed with a 1-2-1 filter to remove potential spurious maxima and minima. Determination of the gap

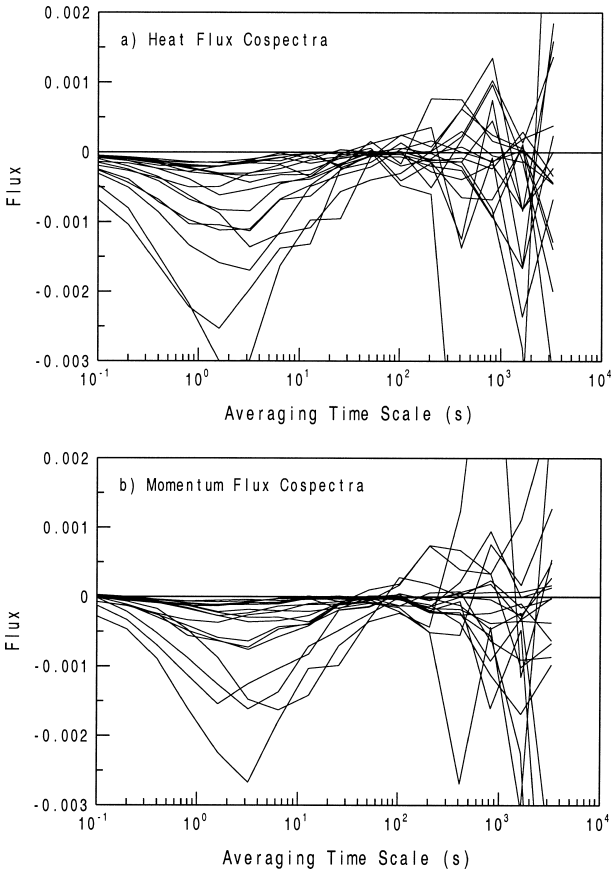

FIG. 3. Averaging timescale dependence of the (a) sonic heat flux (m s^{-1} °C) and (b) alongwind component of the momentum flux (m^2 s^{-2}), for CASES99 5-m sonic data for 18 stable 1-h periods on 12 different nights.

region for individual records was most straightforward for the heat flux, which often changed sign in the gap region. The algorithm for the momentum flux is applied to the magnitude of the stress vector.

For a few periods with very weak turbulence, the gap detection algorithm fails to find any significant peak in the cospectra at scales commonly associated with turbulence. In these cases the cospectra at the shortest averaging timescales are nearly flat and close to zero, indicating that the turbulent flux is zero within measurement error. Our approach was to exclude these cases, and retain an estimate of the cospectral gap only when there was measurable nonzero turbulent flux.

Figure 4 shows the averaging timescale dependence of the fluxes of heat and momentum for a 1-h stable period with a cospectral gap at 30 s. For timescales slightly larger than the gap, the cospectra for both the alongwind component of the momentum flux and the heat flux change sign (Fig. 4a). As a result, the accumulative flux, or equivalently the eddy correlation flux, is a local maximum at the gap scale (Fig. 4b). The accumulative flux for timescale τ is found by summing the contributions to the flux from the shortest timescale

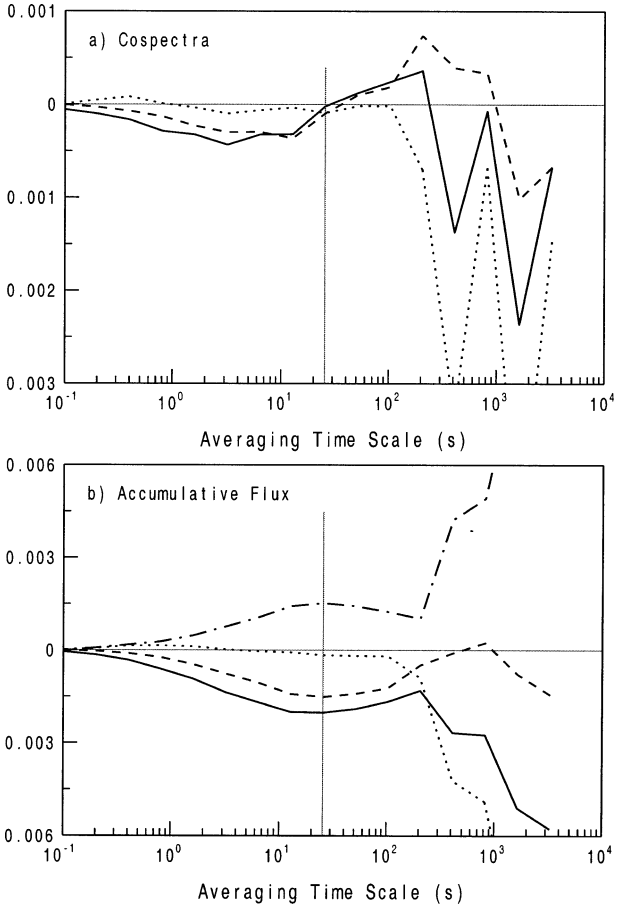

FIG. 4. CASES99 5-m sonic data for one stable period around midnight for the sonic heat flux (solid line), alongwind component of momentum flux (dash), crosswind momentum flux (dots), and magnitude of momentum flux [dash–dot; (b) only] for (a) the cospectra, and (b) the accumulative flux. Vertical line is the gap time scale detected by the algorithm (26 s).

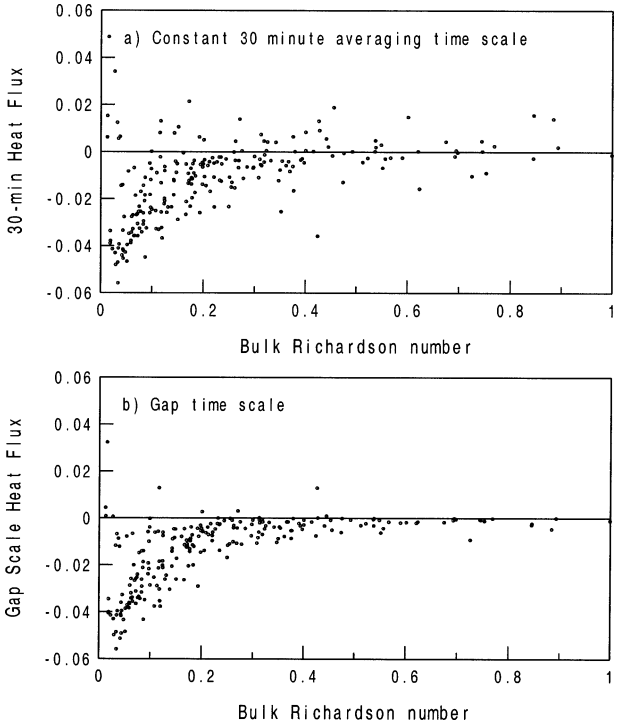

FIG. 5. The 5-m sonic heat fluxes (m s^{-1} °C) vs bulk Richardson number for (a) fluxes calculated using a constant 30-min averaging time and (b) fluxes calculated using the gap timescale.

up to timescale τ. In the region around the gap (20–40-s averaging timescale), the accumulative flux curve is flat, and the flux is not a strong function of averaging time. By contrast, for longer timescales outside the gap region, the accumulative fluxes in this example increase rapidly with increasing averaging time and are highly sensitive to the precise timescale chosen, and therefore are not well posed. At averaging timescales 5 min and longer, the crosswind component of the momentum flux in this example dominates the magnitude of the momentum flux vector. In the small-scale region of the cospectra associated with turbulence, the crosswind component of the momentum cospectra is much smaller than the alongwind component.

Use of the gap timescale from the automated algorithm to calculate the flux does indeed appear to reduce the scatter in stable similarity relationships (Fig. 5). The sonic heat flux calculated using a constant 30-min timescale (Fig. 5a) is counter to the potential temperature gradient in 20% of the stable 1-h periods, while for the identical time periods, the heat flux calculated using the variable gap scale (Fig. 5b) is countergradient only 4% of the time. Upward heat fluxes in stratified conditions are not predicted by similarity theory and here are due to inadvertent capture of poorly sampled mesoscale motions.

One approach for application of this method would be to determine the gap scale for each individual 1-h data record and use that timescale as the averaging timescale in the eddy correlation flux calculation for that particular 1-h period. We chose not to use this approach because the random sampling error in the cospectra for an individual 1-h record is large, especially for the largest averaging timescales that are the most poorly sampled. That is, there is significant random sampling error in an individual 1-h estimate of the gap scale. Instead of this approach, we determine the gap scale for each hour of data for each sonic anemometer and then average the gap scale over the entire experiment to reduce random errors. In the next section, we develop relationships between the averaged gap scale and the height above ground and the bulk stability.

The gap scale estimated from tower data is naturally considered as a timescale since the measurements are made by sampling in time at a fixed location in space. We also calculate a corresponding gap length scale using Taylor's hypothesis (Taylor 1938); however, such a length scale is subject to all the errors associated with application of this hypothesis. Results in this section

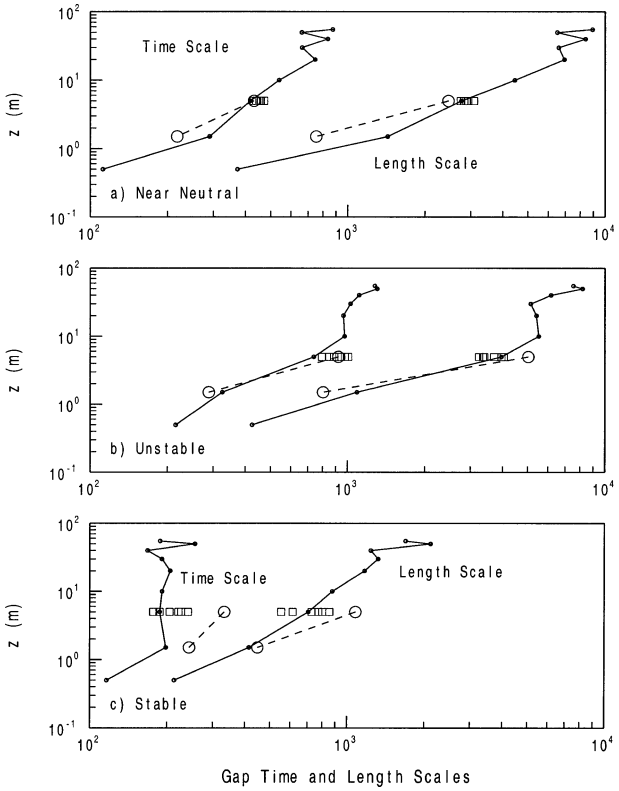

FIG. 6. Height dependence of the composite gap timescale (s) and length (m) scale in CASES99 for the main 60-m tower and UConn tower (solid line and dots), the Iowa flux tower (dashed line and circles), and the six 5-m stations (squares) for (a) near neutral stability, (b) unstable, and (c) weakly stable conditions.

will focus on the gap scale for the CASES99 sonic heat fluxes. The momentum flux cospectra are generally less well behaved than the heat flux cospectra, although the gap timescales for both are similar in neutral and stable conditions. For unstable conditions, the momentum flux gap scale is typically smaller than the heat flux gap scale. This suggests that large convective eddies transport heat more effectively than momentum.

In addition to height above ground and stability, which are the influences we will explicitly consider, the gap scale may also be related to boundary layer depth. Shallow boundary layers could suppress the largest turbulent eddies and reduce the gap scale. At night, the gap scale may be related to the location and intensity of the low level jet, which was commonly observed in CASES99 (Banta et al. 2002). The observations needed to test the boundary layer depth and low level jet influences were not routinely available in our datasets and will not be available in many anticipated applications.

Height and stability dependence

The gap timescale and gap length scale (using Taylor's hypothesis) generally increase with height in near neutral and unstable conditions (Fig. 6). This increase with height is expected due to the presence of the ground, which inhibits the turbulent eddy size. In stable conditions, no clear height dependence of the gap timescale is observed above 1.5 m (Fig. 6c). A possible explanation is that in stable conditions the larger turbulent eddies are limited by the temperature stratification and buoyancy destruction of turbulence such that height above ground becomes a secondary influence. Using Taylor's hypothesis, the gap length scale increases with height in stable conditions due to the increase in the mean wind with height.

While similarity theory provides guidance for the height dependence of the turbulent mixing length and for the peak of the turbulent cospectra, it does not provide any clear guidance for the height dependence of the gap scale separating turbulence and mesoscale motions. For neutral conditions, the mixing length is predicted to increase linearly with height in the surface layer as

$$l_{\text{mix}} \equiv \frac{u_*}{\partial U/\partial z} = \kappa z, \tag{10}$$

where $\kappa \simeq 0.4$ is von Kármán's constant. However, the relationship between the mixing length and the gap scale is not known. Kaimal and Finnigan (1994) found that height dependent cospectra of the momentum flux for the neutral surface layer collapse onto a single curve when viewed as a function of the normalized frequency n, where $n = fz/U$, and f is the dimensional frequency. The interpretation is that the length scale associated with the peak of the turbulent cospectra scales linearly with z. The relationship between the scale of the peak of the turbulent cospectra and the gap scale, however, is not known. In particular, the gap scale can be influenced by the smallest scales of significant mesoscale motion.

We find that the neutral gap length scale does increase approximately linearly with height in the lowest 20 m, but increases at a rate much less than linear above 20 m (Fig. 6a), possibly due to the influences of boundary layer depth. Least squares regression for the neutral gap length scale at 0.5, 1.5, 5, 10, and 20 m above ground in CASES99 gives

$$l_{\text{gap}} = 816\ m + 320z. \tag{11}$$

This relationship explains a substantial fraction of the variance but has two problems: (i) the nonzero intercept (816 m for $z = 0$) is unexpected since in the theoretical limit l_{gap} should approach zero as z approaches zero, and (ii) it grossly overpredicts the gap length scale above 20 m. When interpreting the large asymptotic value at the surface, it must be remembered that the gap scale is the scale that includes all of the turbulent flux and is therefore larger than the scale of the main transporting eddies. This relationship is of more practical value than theoretical value.

A potential reason for the slower increase with height of the neutral gap length scale above 20 m is that a 1-h record may be too short to adequately capture the

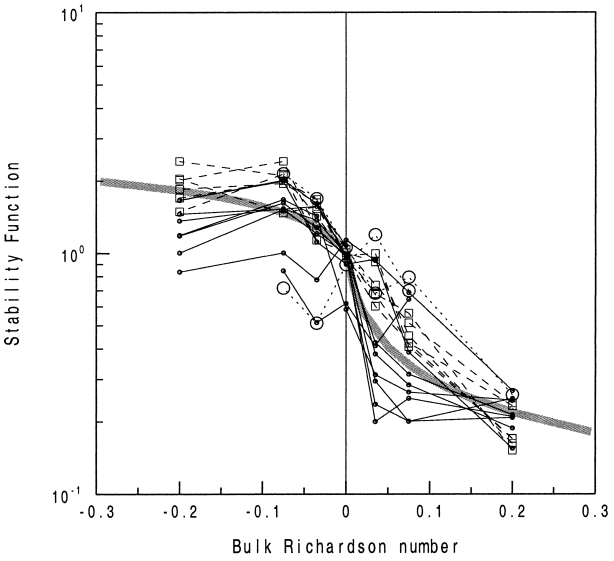

FIG. 7. Stability function $f(R_b)$ in CASES99 for the main and UConn towers (solid lines and dots), the Iowa tower (dotted lines and circles), and the six 5-m stations (dashed lines and squares). The heavy line is a fit to the data [Eqs. (13)–(14)].

larger cospectral gap scales that might be anticipated at these heights. However, after examination of individual cospectra from the highest levels on the tower, it is not obvious that the diagnosed gap scale is limited by the record length. In addition, making our record length longer than 1 h would introduce an unacceptable amount of nonstationarity, conflicting with our goal of improving eddy correlation flux calculations for evaluation of similarity theory.

The turbulence length scale is physically more appealing than the timescale to pass the tower, but to assess the length scale from tower data one needs to assume Taylor's hypothesis. The transformation between time and space has two problems: (i) Taylor's theory may not apply because the eddies do not move with the mean wind speed or they evolve significantly during the time required to pass the tower, and (ii) the eddies generally become more elongated in the wind direction with stronger winds. Given that there is no available alternative, and that we are not attempting to develop a new turbulence theory, we chose to empirically model the gap timescale directly to improve turbulent flux calculations. We select a form for the gap timescale of

$$\tau = \alpha_r (z/z_r)^p f(R_b), \tag{12}$$

where α_r is the neutral gap timescale (seconds) at arbitrary reference height $z_r = 10$ m, and $f(R_b)$ is a stability function equal to unity for neutral flow. The CASES99 neutral data yield $\alpha_r = 540$ s and $p = 1/3$.

Despite considerable scatter between the different sonic anemometers, a good relationship was found between the gap timescale and stability as measured by the bulk Richardson number (Fig. 7). A fit to the stability dependence based on all the CASES99 data is given by

$$f(R_b) = (1 - 50R_b)^{1/4}; \qquad R_b < 0 \tag{13}$$

$$f(R_b) = (1 + 100R_b)^{-1/2}; \qquad R_b > 0, \tag{14}$$

where the stability function was found by first removing the neutral height dependence. Some of the scatter in Fig. 7 is due to the stability dependence of the height dependence, which for simplicity has been excluded from the model. The coefficients for $f(R_b)$ may be sensitive to the levels used to calculate the gradients in the bulk Richardson number. For extreme positive or negative bulk Richardson numbers, where $f(R_b)$ either vanishes or becomes very large, we constrain the gap timescale to be no smaller than 30 s and no larger than 1200 s.

The gap scale model is applied to the calculation of eddy correlation fluxes as follows. The bulk Richardson number is estimated from the 1-h average wind speed and the 1-h average temperatures [Eq. (9)]. The gap timescale is evaluated using the height and stability-dependent model [Eqs. (12)–(14)]. Quantities such as the vertical velocity w and temperature T are decomposed into a mean and a fluctuating part, as in standard Reynold's decomposition, using the gap timescale to define the local averaging time and therefore the fluctuations (e.g., w' and T'). The fluxes (e.g., $w'T'$) are then averaged over 1 h to reduce random sampling errors.

We now test the generality of the model for the cospectral gap timescale based on CASES99 data by comparing to the auxiliary datasets, which were not consulted in developing the model. For the comparison, gap timescales within a factor of 2 represent good agreement since the calculated fluxes are usually not sensitive to the precise timescale as long as the timescale is in the gap region, where the accumulative flux is not changing rapidly with averaging scale. We find good general agreement for the other datasets (Fig. 8), with the possible exception of the 2-m sonic in BORRIS95, where the stability dependence is weaker than the other datasets. The bulk Richardson number in MICROFRONTS was small compared to CASES99 due to stronger winds and more frequent cloudy conditions. For near neutral conditions, the gap scale for 10-m MICROFRONTS data (800 s) is larger than the model based on CASES99 (540 s). For BORRIS95, the three highest measurement levels are in general agreement with the model, and the height dependence for near-neutral conditions was similar to that found for CASES99 and MICROFRONTS. We conclude that the auxiliary datasets generally support the conclusions based on CASES99 data.

5. Implications for similarity theory

The expectation of applying the gap scale model to calculate fluxes is that the fluxes will better represent turbulent transport and be more tightly coupled to the local wind shear and temperature stratification. That is, the scatter in similarity relationships should be reduced

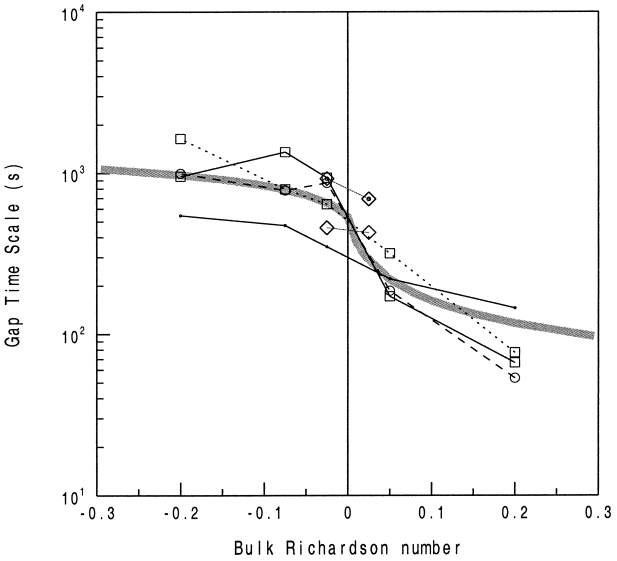

FIG. 8. Stability dependence of the gap timescale for BORRIS95 data at levels of 2 (solid dot), 7 (dash circle), 10 (dotted square), and 20 m (solid square), and for MICROFRONTS data at levels of 3 (diamond) and 10 m (diamond–dot). The heavy line is the model based on the CASES99 data for $z = 10$ m.

using the gap scale fluxes. This result is not guaranteed however because the model [Eqs. (12)–(14)] is based on the average gap timescale for 16 sonic anemometers in CASES99, and there is considerable scatter in the gap timescale for a given height and stability. Some of the scatter is probably due to the different height dependence of the gap scale for different stabilities. It is not clear what the systematic influence on the magnitude of the fluxes will be, since the flux at scales larger than the turbulence does not appear to be predictable. In this section, we will focus on the measurements made at and below 10 m above ground in CASES99. We will address the systematic influence on the fluxes first and then examine scatter in similarity relationships.

Averaging over the entire experiment, the friction velocity u_* increases slightly with increasing averaging timescale (Table 2). These friction velocities are calculated as the square root of the magnitude of the momentum flux vector. For unstable conditions, the friction velocities are larger (0.9%) when using a 30-min timescale compared to using the gap scale model, and smaller (1.4%) when using a 5-min timescale compared to the gap model. For stable conditions, where the gap model timescale ranges from a few minutes down to 30 s, the gap scale u_* is smaller than the 5-min u_*, which is smaller than the 30-min u_*, when averaged over the entire experiment. One factor responsible for the systematic increase in u_* with averaging time is the increase in the crosswind component of the momentum flux with averaging time (e.g., Fig. 4). Since u_* is calculated as a magnitude from two components, a crosswind stress of either sign increases u_*. The directional shear of the mean wind observed at the main tower was typically small, indicating that the crosswind stress is probably not related to the mean local shear, but possibly is due to larger-scale (mesoscale) meandering of the wind and possible momentum transport by gravity waves.

Small but systematic differences were also found for the sonic heat fluxes (Table 2). During daytime convective periods, the upward heat flux increases with increasing averaging timescale such that heat fluxes based on 30-min averages are slightly greater (1.3%) than the gap scale heat fluxes, which use an averaging time of 20 min or less. Larger upward heat fluxes normally improve the surface energy budget. In fact, Sakai et al. (2001) recommend using an averaging time of several hours for convective conditions to balance the surface energy budget. Here the intention is to include only the turbulent heat flux. For stable conditions, the systematic heat flux difference is small although there is large scatter between the different sonic anemometers (Table 2).

To test whether the scatter in similarity relationships can be reduced for the CASES99 stable dataset, we calculated the stability parameter z/L, where L is the Obukhov length scale:

$$L = -\frac{u_*^3}{\overline{w'\theta_v'}(g/\theta)\kappa}. \tag{15}$$

The Obukhov length is a function of the momentum flux (u_*^2) and the virtual heat flux ($\overline{w'\theta_v'}$) (or sonic heat flux), and therefore depends on the averaging timescale used to calculate the fluxes. For stable conditions, higher correlation between z/L and the bulk Richardson number [Eq. (9)] would be associated with less scatter in similarity relationships.

For stable conditions, z/L calculated using the model

TABLE 2. Percent difference in mean fluxes averaged over the entire experiment for comparing systematic differences in fluxes calculated using a constant 30-min and 5-min averaging timescale to fluxes calculated using the gap scale model. The range and mean are for 9 different sonic anemometers below 10 m in CASES99. The data were partitioned into two stability categories based on the sign of the heat flux.

	Unstable			Stable		
	Min	Max	Mean	Min	Max	Mean
u_* 30-min minus gap	0.3	1.7	0.9	1.1	4.2	2.5
u_* 5-min minus gap	−2.8	−0.1	−1.4	−0.4	1.1	0.5
$\overline{w'T'}$ 30-min minus gap	0.7	1.9	1.3	−3.2	4.6	1.3
$\overline{w'T'}$ 5-min minus gap	−4.6	−0.8	−2.7	−3.9	1.8	−0.3

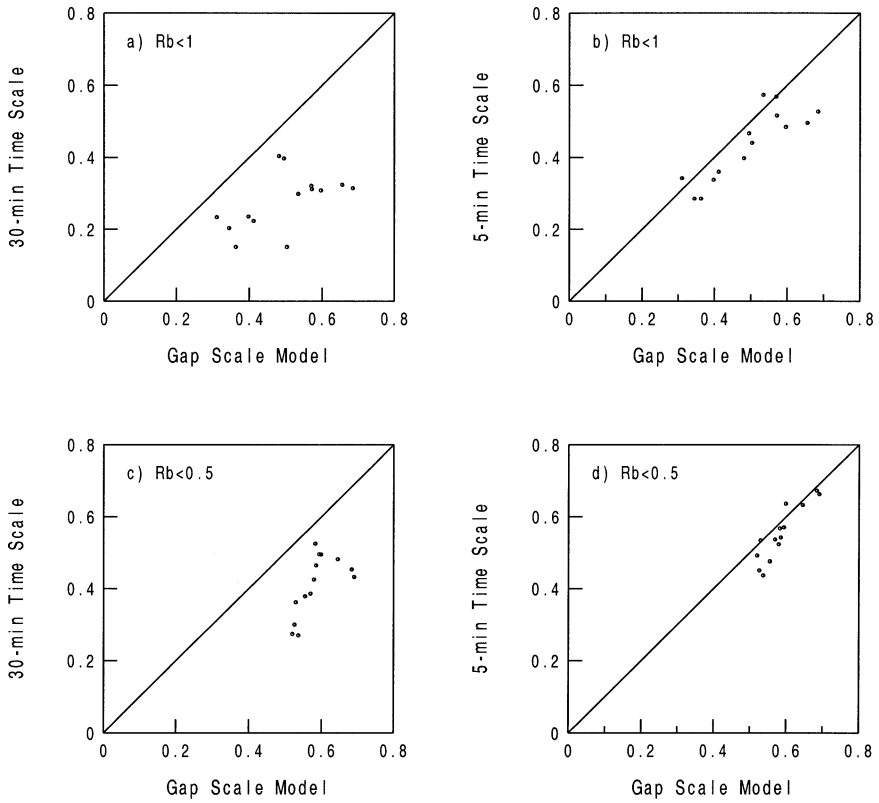

FIG. 9. Correlation coefficient between z/L and R_b for 14 sonic anemometers in CASES99 stable conditions for (a) 30-min averaging time vs gap model for $R_b < 1$, (b) 5 min vs gap model for $R_b < 1$, (c) 30 min vs gap model for $R_b < 0.5$, and (d) 5 min vs gap model for $R_b < 0.5$.

gap scale is indeed more highly correlated with bulk stability than when calculated using a 30- or 5-min timescale (Fig. 9). Averaging the correlation coefficients for the 14 sonic anemometers in Fig. 9 for conditions with $0 < R_b < 1$, the correlation coefficient increases by a factor of 1.8 (1.2) using the gap scale model compared to using a 30- (5-) min timescale. In the calculations for Fig. 9, we have excluded a few outliers with near zero momentum flux where the 1-h average z/L was <-5 or >10.

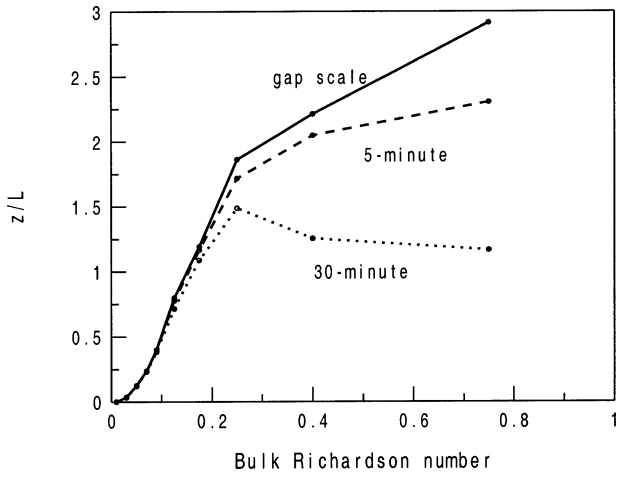

FIG. 10. Bulk Richardson number dependence of z/L for fluxes calculated using the gap timescale model (solid), a constant 5-min timescale (dashed), and a 30-min timescale (dot). The data include 8 different sonic anemometers at or below 5 m in CASES99.

Regardless of which timescale is used to calculate the fluxes, the correlation between z/L and R_b for stable conditions decreases with height on the tower (not shown). This is probably due to shallow stable boundary layers where the fluxes in the top half of the tower layer become partially decoupled from the bulk stability below 15 m, as represented by R_b. Mahrt and Vickers (2002) found that thin stable boundary layers of depth 30 m or less were commonly observed in CASES99. In these conditions, the surface layer where similarity theory applies becomes very shallow (a few meters) and most of the measurement heights are above the surface layer.

Use of the gap scale model systematically increases the estimate of the stability parameter z/L for the strongest bulk stability conditions (Fig. 10). In Fig. 10 we have grouped 1-h values of z/L by R_b category and then averaged over the entire experiment. These averages were then composited for the lower-level sonic anemometers. For strong stratification and weak winds, z/L decreases as the averaging timescale used to calculate the fluxes

increases. For a 30-min timescale and strong stability ($R_b > 0.25$), the mean z/L decreases with increasing R_b, contrary to expectations. This result does not seem physical and is due to erroneous inclusion of flux at larger scales. By comparison, for the 5-min and the gap scale fluxes, z/L increases with increasing bulk stability over the entire range of stability.

Heat fluxes that are directed counter to the local temperature gradient are not predicted by similarity theory and contribute to scatter when evaluating similarity relationships. Compared to using a fixed 30-min timescale, employing the gap scale model reduced the number of time periods with countergradient heat fluxes by a factor of 2–5, depending on the level and sonic anemometer considered. These calculations include the entire CASES99 dataset.

We now examine the influence of the averaging timescale used to calculate the fluxes on the stability dependence of the drag coefficient. Similarity theory predicts that the drag coefficient is a function of z/L and z/z_o,

$$C_d = \left[\frac{\kappa}{\log(z/z_o) - \psi_m}\right]^2, \tag{16}$$

where z_o is the aerodynamic roughness length and $\psi_m(z/L)$ is the stability function for momentum. We use a constant aerodynamic roughness length of 3 cm for CASES99 based on calculations for near-neutral conditions, and the form of ψ_m given by Paulson (1970) and Businger et al. (1971) for unstable conditions. For stable conditions, we use $\psi_m = -5z/L$ after Dyer (1974). The function ψ_m is positive for z/L less than zero (unstable), and negative for z/L greater than zero (stable), such that the drag coefficient is augmented relative to the neutral value in unstable conditions and reduced relative to the neutral value in stable conditions. In the surface layer with Monin–Obukhov similarity, the height dependence of the fluxes is neglected while the mean wind speed increases with height such that C_d always decreases with height. The drag coefficient is calculated from data as $C_d = (u_*/U_z)^2$. The stability parameter z/L and the friction velocity u_* are dependent on the averaging time scale used to calculate the fluxes.

The observed and predicted stability dependences of the drag coefficient for 5- and 10-m sonic anemometer data in CASES99 are shown in Fig. 11. The mean unstable C_d from the gap scale fluxes is closer to the prediction than is C_d calculated using either the 5- or 30-min fluxes. The decrease in C_d with increasing instability for some ranges of negative z/L for the 5- and 30-min flux sets in Fig. 11 does not seem physical and is not predicted by similarity theory. This behavior occurs in the stable nocturnal boundary layer where R_b is positive yet the heat flux calculated using a 5- or 30-min averaging time is upward, thus falsely indicating unstable conditions and negative z/L. The heat fluxes calculated using a 5- or 30-min averaging time scale are upward due to erroneous inclusion of flux at scales larger than the turbulence. The gap model timescale for these periods is typically 1 min, and the gap scale heat flux is downward, consistent with the temperature stratification and the small values of the drag coefficient. Use of a time scale greater than a few minutes in these conditions can lead to small C_d at large negative z/L, contrary to the similarity prediction and physical expectations.

6. Conclusions

Multiresolution cospectra of the heat and momentum fluxes generally identifies a gap region that separates turbulent and mesoscale transport, especially in the stable boundary layer, where gap timescales of a few minutes or less are commonly observed. We develop a simple model for the gap timescale as a function of height above ground and bulk atmospheric stability to provide guidance in choosing the averaging timescale that defines the fluctuations for eddy correlation flux calculations. Regardless of the gap timescale, we average the fluxes (products of fluctuations) over a 1-h period to reduce random flux sampling errors. The gap scale fluxes are an improvement over fluxes calculated using a constant averaging time in the sense that they lead to less scatter in similarity relationships. Including mesoscale transport in calculated fluxes can degrade similarity relationships. An estimate of the bulk Richardson number is required for application of the model. The model does not include any potential influence on the gap scale due to boundary layer depth since such information is not routinely available in many applications.

A model of the gap timescale was developed from a large tower dataset that includes 16 sonic anemometers deployed for a 1-month period. The model compares favorably with two other smaller independent datasets that were also over a relatively flat homogeneous surface with low vegetation. Because the gap scale is influenced by the degree of mesoscale activity, the gap timescale may be different at sites not tested here. In particular, local circulations due to terrain and surface heterogeneity could enhance mesoscale motion and lead to a smaller gap scale compared to the more homogeneous case.

The gap timescale generally increases with height in the lowest 50 m due to the presence of the ground which inhibits the turbulent eddy size. In stable conditions, where the temperature stratification limits the turbulence, the gap scale is more nearly independent of height. The gap timescale increases with instability due to augmentation of the large eddies by convection, and decreases with stability due to suppression of the large eddies by the stratification. For neutral conditions at 10 m above ground, the average gap timescale is 9 min. The gap scale decreases sharply with increasing stability

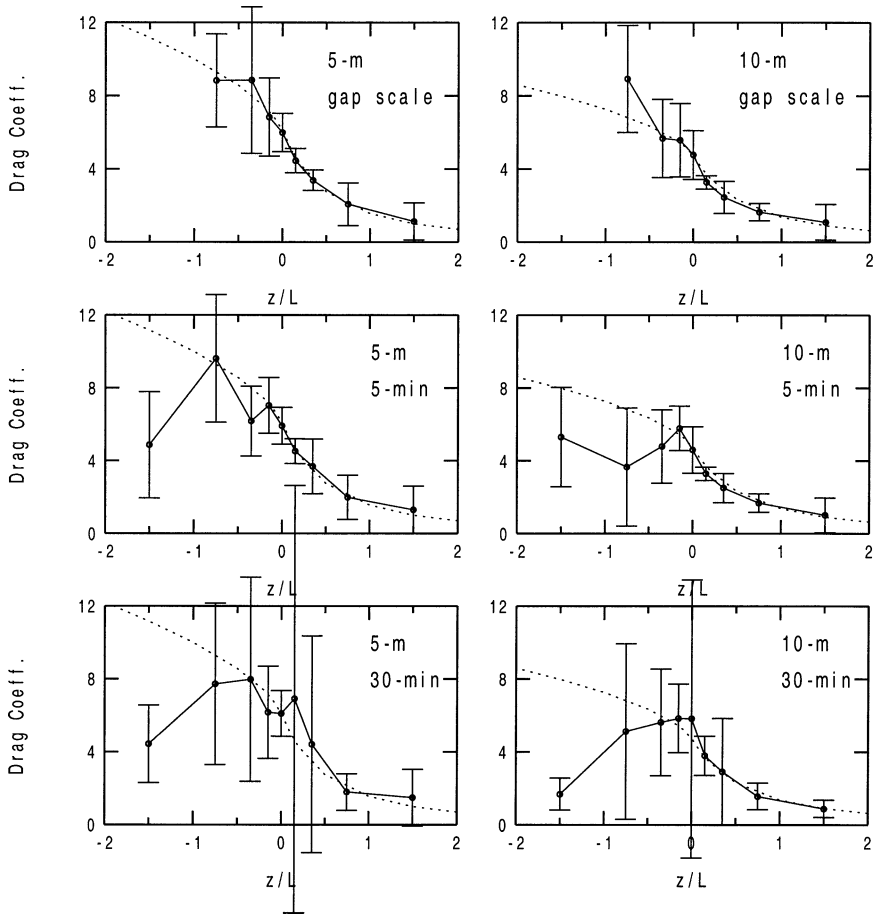

FIG. 11. Stability (z/L) dependence of the drag coefficient ($C_d \times 1000$) for fluxes calculated using (top) the gap timescale model, (middle) a 5-min averaging time, and (bottom) a 30-min averaging time to define the fluctuations for the (left) 5-m UConn sonic and (right) the 10-m sonic on the main tower in CASES99. Error bars show plus/minus one standard deviation. Dashed line is the similarity theory prediction.

to 100 s for strong stability ($R_b = 0.25$). For the strongest stratification and weakest wind speed cases, where R_b becomes large, we do not allow the gap timescale to be smaller than 30 s. A clear gap region was not always evident for unstable conditions where large convective eddies and mesoscale motions overlap.

Use of the variable averaging timescale, as compared to the common approach of using a constant averaging timescale, reduces the scatter in stable boundary layer similarity relationships as measured by the correlation between R_b and z/L. The scatter is reduced by excluding mesoscale contributions to the calculated fluxes. These mesoscale fluxes are typically not related to the local wind shear or temperature stratification in a systematic way and are poorly sampled.

In stable conditions, fluxes calculated using the short averaging time of the gap model lead to systematically larger values of the stability parameter z/L. This is primarily due to a smaller estimate of the friction velocity for the shorter averaging time (a few minutes or less) of the model. The momentum fluxes at scales larger than the gap scale are commonly dominated by the crosswind component, even when there is little directional shear of the mean wind. The crosswind component of the stress is associated more with large scale meandering of the wind and possibly gravity waves than with turbulence.

Numerous cases are found where the heat flux calculated using a timescale as short as 5 min is upward in the stably stratified boundary layer, contrary to the similarity prediction. For these same cases, the heat flux cospectra clearly show downward flux at shorter timescales. Use of the gap scale captures the downward heat flux at short timescales by excluding the upward flux at longer timescales. This significantly reduces the number of countergradient heat flux cases. Use of the adjustable averaging timescale reduces the scatter in the z/L dependence of the drag coefficient. Fixed averaging timescales can lead to an erroneous decrease in the mean drag coefficient with increasing instability due to the incorrect sign of the heat flux resulting from contamination by mesoscale motions.

Acknowledgments. We gratefully acknowledge the field assistance of the NCAR ATD staff and Jielun Sun and Sean Burns. This material is based on work supported by Grant DAAD19-0210224 from the Army Research Office and Grant 0107617-ATM from the Physical Meteorology Program of the National Science Foundation.

REFERENCES

Banta, R., R. Newsom, J. Lundquist, Y. L. Pichugina, R. L. Coulter, and L. Mahrt, 2002: Nocturnal low-level jet characteristics over Kansas during CASES-99. *Bound.-Layer Meteor.,* **105,** 221–252.

Businger, J. A., J. C. Wyngaard, Y. zumi, and E. F. Bradley, 1971: Flux profile relationships in the atmospheric surface layer. *J. Atmos. Sci.,* **28,** 181–189.

Dyer, A., 1974: A review of flux-profile relationships. *Bound.-Layer Meteor.,* **7,** 363–372.

Haar, A., 1910: Zur theorie der orthogonalen funktionensysteme. *Math. Ann.,* **69,** 331–371.

Howell, J. F., and L. Mahrt, 1997: Multiresolution flux decomposition. *Bound.-Layer Meteor.,* **83,** 117–137.

——, and J. Sun, 1999: Surface-layer fluxes in stable conditions. *Bound.- Layer Meteor.,* **90,** 495–520.

Kaimal, J. C., and J. J. Finnigan, 1994: *Atmospheric Boundary Layer Flows: Their Structure and Measurements.* Oxford University Press, 289 pp.

Katul, G., and B. Vidakovic, 1996: The partitioning of attached and detached eddy motion in the atmospheric surface layer using Lorentz wavelet filtering. *Bound.-Layer Meteor.,* **77,** 153–172.

Mahrt, L., 1998: Flux sampling strategy for aircraft and tower observations. *J. Atmos. and Oceanic Technol.,* **15,** 416–429.

——, and D. Vickers, 2002: Contrasting vertical structures of nocturnal boundary layers. *Bound.-Layer Meteor.,* **105,** 351–363.

——, X. Lee, A. Black, H. Neumann, and R. M. Staebler, 2000: Nocturnal mixing in a forest subcanopy. *Agric. For. Meteor.,* **101,** 67–78.

——, E. Moore, D. Vickers, and N. O. Jensen, 2001: Dependence of turbulent and mesoscale velocity variances on scale and stability. *J. Appl. Meteor.,* **40,** 628–641.

Mallat, S. G., 1989: The theory of multiresolution signal decomposition: The wavelet representation. *IEEE Trans. Pattern Anal. Mach. Intell.,* **7,** 674–693.

Paulson, C. A., 1970: The mathematical representation of wind speed and temperature profiles in the unstable atmospheric surface layer. *J. Appl. Meteor.,* **9,** 857–861.

Poulos, G. S., and Coauthors, 2002: CASES-99: A comprehensive investigation of the stable nocturnal boundary layer. *Bull. Amer. Meteor. Soc.,* **83,** 555–581.

Sakai, R. K., D. R. Fitzjarrald, and K. E. Moore, 2001: Importance of low-frequency contributions to the eddy fluxes observed over rough surfaces. *J. Appl. Meteor.,* **40,** 2178–2192.

Smedman, A. S., 1988: Observations of multi-level turbulence structure in a very stable atmospheric boundary layer. *Bound.-Layer Meteor.,* **44,** 231–253.

——, and U. Högström, 1975: Spectral gap in surface-layer measurements. *J. Atmos. Sci.,* **32,** 340–350.

Stull, R. B., 1990: *An Introduction to Boundary Layer Meteorology.* Kluwer Academic, 666 pp.

Sun, J., and Coauthors, 2002: Intermittent turbulence associated with a density current passage in the stable boundary layer. *Bound.-Layer Meteor.,* **105,** 199–219.

Taylor, G., 1938: The spectrum of turbulence. *Proc. Roy. Soc. London,* **A164,** 476–490.

Vickers, D., and L. Mahrt, 1997: Quality control and flux sampling problems for tower and aircraft data. *J. Atmos. Oceanic Technol.,* **14,** 512–526.